PARAMETRIC STUDY OF INJECTION CONDITIONS WITH CO-AXIAL INJECTION OF GASEOUS HYDROGEN AND LIQUID OXYGEN

S. Webster, J.Hardi, M. Oschwald.
DLR- German Aerospace Center, Institute of Space Propulsion, Lampoldshausen, Germany, D-74239

Abstract

High frequency instability is an on going danger to the successful operation and development of new liquid propellant rocket engines. The highly destructive nature of high frequency instability can result in safety risks and costly delays in engine development programs. Further understanding of the mechanisms and parameters that affect combustion stability can be used to further limit these dangers. The rectangular combustor designated 'BKH' was developed to study flame-acoustic interaction under forced excitation for both sub and super critical conditions. This paper presents a preliminary parametric study undertaken during run in testing of the new 'BKH' hardware. The focus is on the affects of oxidizer to fuel ratio and velocity ratio on the roughness of combustion for warm GH2 at sub and super critical pressures. It was found that higher injection velocity ratio increased the energy content of high frequency acoustic energy for warm GH2 and that higher oxidizer to fuel ratio produced less combustion roughness. This trend is inconsistent with observations presented by Wanhainen et al (1966).

1. INTRODUCTION

High frequency (HF) combustion instability when oscillating with one or more of the natural acoustic resonances of a combustion chamber can rapidly form highly destructive pressure oscillations [1, 2]. Testing and re-design of full scale flight engines after experiencing high frequency combustion instability is a costly and time consuming activity. In an effort to mitigate these risks at a reduced cost, subscale rocket combustors are used to investigate the driving mechanisms of high frequency combustion instability. Specifically, the aim is to mitigate high frequency combustion effects through improved guidelines for the development of combustion engines and insight into the driving mechanisms of high frequency instability.

To this end the combustion chamber designated ''BKH'' (Brennkammer H) was developed. 'BKH' includes the possibility of external forcing as initially presented by Lecourt and Foucaud (1987) [3]. This concept has now been applied to a number of sub scale combustors both in Germany (CRC) and in France (CRC, MIC) and has been shown to be effective in forcing high frequency pressure oscillations on a combustion chamber [4, 5]. However, the investigations presented in this paper will focus on effects of injection parameters on combustion roughness without external forcing.

Wanhainen et al (1966) [6] established a set of injection parameter guidelines for which co-axial shear injection of liquid oxygen and hydrogen were found to be stable. The criteria chosen for investigation and the investigation procedure were based on the destabilizing effect of cold hydrogen observed during the J-2 development program. Wanhainen et al (1966) established thorough temperature ramping generalized trends for stability as well as specific stability margins for the combustion chamber used in the investigation. In particular the oxidizer to fuel ratio and injection velocity ratios were investigated through a range of hardware and operational parameter changes. It was shown that lower oxidizer to fuel ratios resulted in lower hydrogen temperatures before the triggering of high frequency instability and thus are considered more stable. It was also shown that for the combustion chamber used an injection velocity ratio greater than 6.5 was stable independent of hydrogen injection temperature.

The goal of the following paper is to investigate 'BKH' for stability relationships in the ambient temperature (~290° k) GH2 operational domain. As 'BKH' uses the shear coaxial injection method and is operated with hydrogen and oxygen as was the case presented by Wanhainen et al (1966) comparison is made between the two results.

No temperature ramping such as that undertaken by Wanhainen et al (1966) is used. Therefore an alternative method for measuring the stability of the combustion chamber is required. The root mean squared method (RMS) for measuring the energy of an oscillating signal is a well-established method. Thus the RMS of the dynamic pressure signal is used to rate the stability of the system for a range of operating and injection conditions. In particular, the oxidizer to fuel ratio such as investigated by Wanhainen et al (1966), the injection velocity ratio and the momentum flux ratio were investigated.

2. METHODS AND MATERIALS

2.1. Hardware

The combustion chamber designated 'BKH' was used for the collection of all experimental results. A brief overview of 'BKH' and associated experimental apparatus are presented here. However, for more detail readers are directed to Hardi et al (2011)[7].

2.1.1. Combustion Chamber

'BKH' is a combustion chamber with a rectangular cross section. Injection of propellants is in the axial direction following the mean flow from the injector to the main

nozzle located directly opposite the injector.

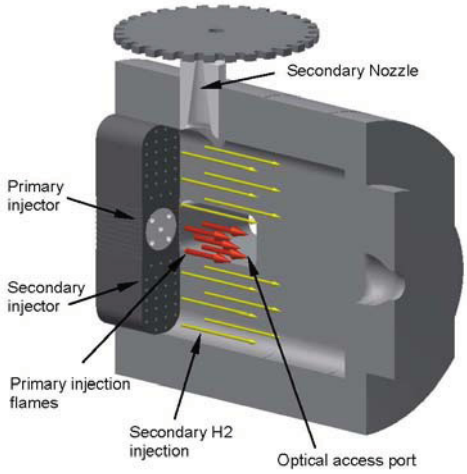

Figure 1. Visualization of 'BKH' combustion chamber design.

The dimensions of 'BKH' (length; L_x=305mm, width; L_y=50mm and height; L_z=200mm) were selected so that the fundamental acoustic resonance frequencies would be close to those which occur in a typical upper stage rocket engine. Dimensions similar to those used in flight hardware are required if the time scales over which the acoustic filed oscillates are to be representative of self sustaining combustion instabilities in real world launch systems. This is important as the interaction between the acoustic field and injection, atomization, vaporization, mixing and combustion processes were established by Heidmann & Wieber (1966) as frequency sensitive [8].

2.1.2. Combustion Chamber Acoustics

Acoustic frequencies of a combustion chamber are those frequencies at which natural pressure oscillations form a standing wave.

For complicated geometries it is not possible to calculate an analytical solution. In these cases a finite element (FE) method is required. For our purposes the solutions of the 1T, 1L and first secondary dome mode using the FE model described by Hardi et al (2011) are visualized in Figure 2.

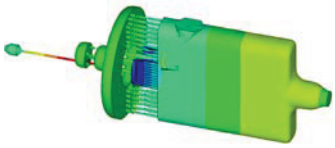

(a)

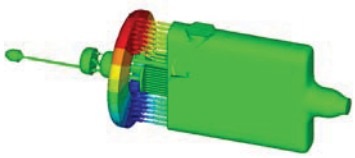

(b)

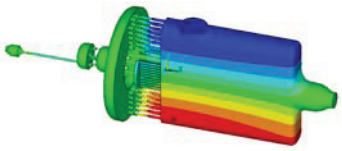

(c)

Figure 2. Visualisation of relevant 'BKH' acoustic modes; (a) first longitudinal mode (1L), (b) secondary hydrogen dome first rotational mode (1R) and (c) first tangential mode (1T) [7].

Figure 3 presents a fast Fourier transform of the high frequency signal for the frequency range of interest. The large peak observed near the 1L mode was identified as originating in the secondary hydrogen dome with its orientation shown in Figure 2(b). Furthermore, a frequency peak lower than the 1L mode was identified as a sensor artefact resulting in a non physical result [7].

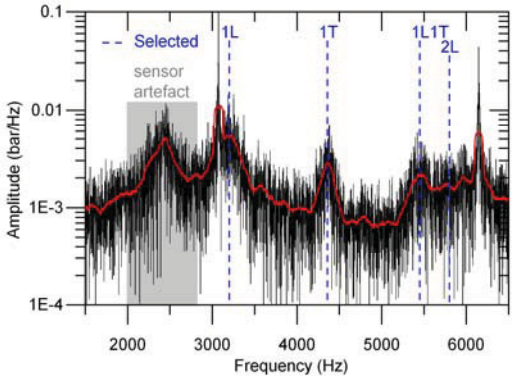

Figure 3. Acoustic high frequency spectra from 1500 to 6500 Hz [7].

2.1.3. Operation

The data collected for this investigation was the result of two separate test campaigns conducted on the European test facility P8 at Lampoldshausen Germany. The first of which was carried out with contributions from the secondary dome to the combustion chamber frequency spectra and the second after the inclusion of the secondary dome baffle which eliminated these contributions. In both cases 'BKH' was operated at ambient conditions for hydrogen (~290K) and cryogenic temperatures for oxygen (~125K). Although separate campaigns both were operated at similar ambient temperature conditions and thus the temperature operational domain is comparable.

2.2. Analysis Techniques

This investigation was designed to complement previous investigations of 'BKH' acoustic spectra such as that presented by Hardi et al (2011). The use of RMS and filtering techniques to investigate the signal allows real value results to be compared with peak power estimates from spectral fast Fourier transform analysis. In addition using RMS methods allows direct comparison between real chamber pressure values (P'rms) and injection

conditions.

2.2.1. Decomposition of Data for investigation

The convoluted nature of the frequency spectra presented in Figure 3 requires that the high frequency pressure data used for RMS investigation is first decomposed into individual frequency contributions.

For this purpose a filter was applied to the signal in the frequency domain before returning the data to the time domain for RMS investigation. This frequency cut off filter was used due to its high resolution frequency cut off rate allowing accurate removal of closely spaced unwanted frequency contributions. The downside to such filtering methods is they are non causal and the original data set cannot be recovered once the filter has been applied.

To investigate the effects of injection conditions on specific chamber modes and on the overall spectrum with out the contribution from both the sensor artifact and dome mode contributions five filters were applied. Table 1 contains the frequency range over which each of the three primary investigations was filtered.

Investigative Goal	Lower cutoff frequency	Upper cutoff frequency	Other removed contributions
High Frequency Domain	1000 Hz	50000 Hz	2000-2600 Hz – Sensor artifact 30 Hz either side of secondary hydrogen dome mode and first overtone.
First Longitudinal mode (1L)	2900 Hz	3400 Hz	30 Hz either side of secondary hydrogen
First Tangential mode (1T)	3950 Hz	4450 Hz	NA

Table 1. Frequency domains for RMS investigation

2.2.2. Calculation of Root Mean Squared

A calculation of the root mean square was undertaken for each of the dynamic pressure data sets after the application of the required filters according to Equation 1.

$$P'rms = \sqrt{\frac{\sum_{1}^{N} x_n^2}{N}} \qquad (1)$$

Each data period under investigation varied from 0.1 to 2 seconds duration for which the test operating point (temperature, pressure, and mass flow rate) was held constant. The RMS was then calculated for 700 data point windows at the sampling rate of 100,000 Hz which results in a data point for every 0.007 seconds of data. The windowing length was chosen to remove the susceptibility of the method to very short time combustion effects and focus on those related to the injection conditions. A 50% window overlap was also included. The mean and standard deviation of the entire period was then calculated. Figure 5 shows an example of the calculated RMS for a sample window along with its mean and standard deviation.

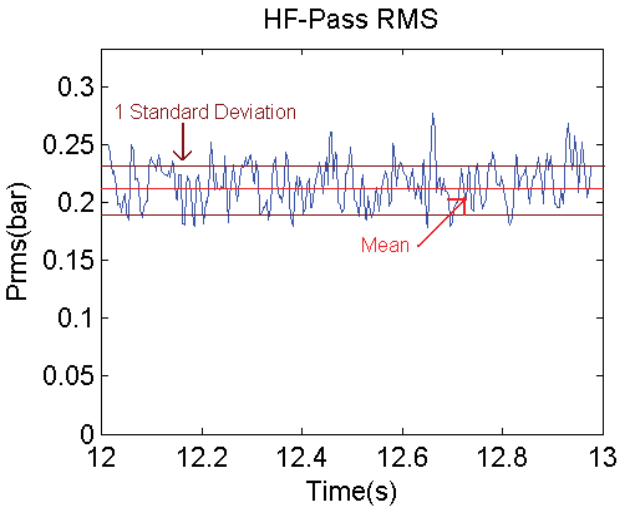

Figure 5. Dynamic pressure (P'_{rms}), standard deviation and mean.

When plotting the P'_{rms} against injection condition values the P'_{rms} was normalized by representing it as a percentage of combustion chamber pressure (P_{cc}).

2.3. Discussion of error

Error estimation for the values presented in the following scatter plots was undertaken in one of two ways.

In the case for injection parameter estimation sensor accuracy after calibration testing as well as known certainty limits on test bench mass flow rates was used. In the cases where a combination of sensor values was required (for example temperature for calculation of density) the error was estimated using standard propagation of errors methodology and worst case values when look up tables were used (such as those for density).

For error estimation of dynamic pressure sensor data two standard deviations were taken as the error bar contribution to provide a 95% confidence interval when a Gaussian distribution is assumed. They were then combined with sensor accuracy limits using standard propagation of error methods.

The final result is that the size of the error bars for the dynamic pressure energy are significant and in the case where only a small frequency band with low energy content is investigated the error bars can be greater than ± 50% of the energy value. It is unlikely that these values can be improved upon and must be accepted as an indication of the complicated processes under investigation.

3. RESULTS AND DISSCUSSION

Wanhainen et al (1966) focuses on two major relationships, the ratio of oxidizer to fuel (O/F) and the

affect of injection velocity on screech (high frequency instability). The work presented here will also focus on the same relationships. However, all tests were conducted with the same hardware including injection elements and thus complete separation of injection condition related effects is impossible.

3.1. Effect of Oxidizer to Fuel Ratio

Figure 6 shows the relationship between oxidizer (liquid oxygen) to fuel (hydrogen) ratio of the primary injector and the normalized dynamic pressure RMS in the high frequency domain (Table 1). Overall the system is very stable showing oscillations of around only 0.2% of combustion chamber pressure. The data points presented range from sub to super critical pressures for oxygen and for a range of oxidizer to fuel ratios relevant to real world rocket applications.

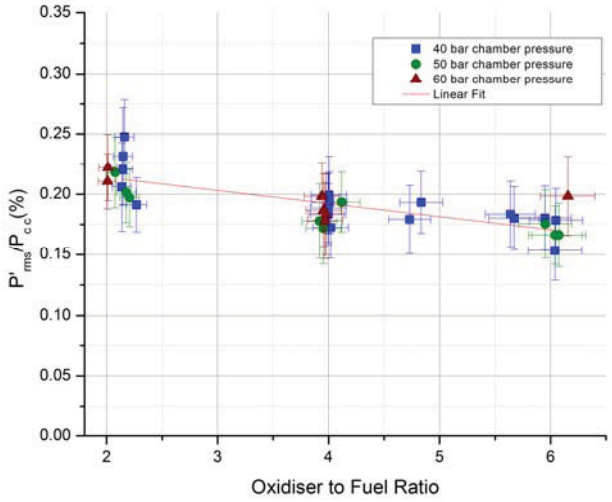

Figure 6. Oxidizer to fuel ratio vs. normalized dynamic pressure RMS over the high frequency domain

A line of best fit has also been applied and suggests a negative relationship between chamber stability and oxidizer to fuel ratio. The line was found to have a significance (with respect to t-test methodology) of greater than 95% with the null hypothesis taken as a line of zero gradient (no relationship). However, the line of best fit also resulted in a mediocre adjusted R^2 value (0.56) suggesting that there is a significant proportion of noise in the signal. This is unsurprising given the significant error bars and relatively low dynamic pressure readings with respect to combustion chamber pressure.

The effects of oxidizer to fuel ratio on specific frequency bands was also investigated, in particular the effect of oxidizer to fuel ratio on the first longitudinal and the first tangential combustion chamber modes. These are presented in Figure 7 and Figure 8 respectively.

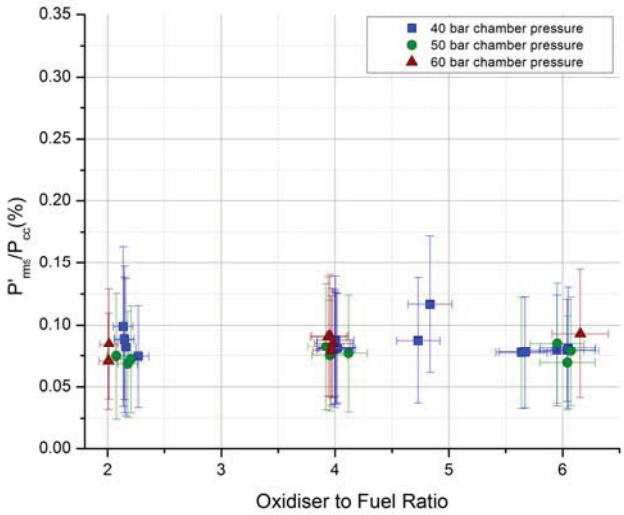

Figure 7. Oxidizer to fuel ratio vs. normalized dynamic pressure RMS for the first longitudinal mode

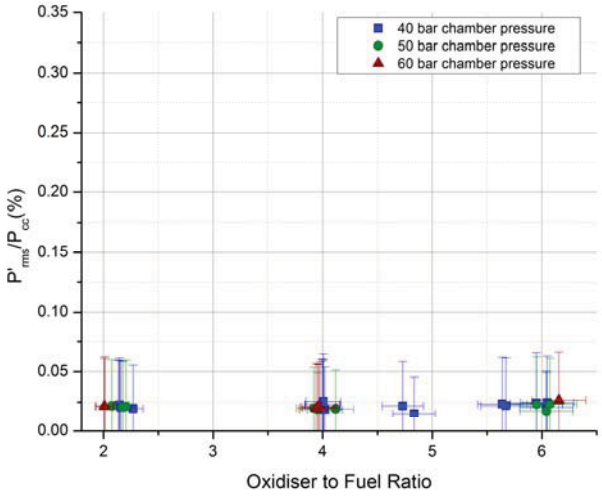

Figure 8. Oxidizer to fuel ratio vs. normalized dynamic pressure RMS for the first tangential mode

As expected the normalized P'_{rms} is greatly reduced for both cases and in both cases it is clear that there is no dependence on the oxidizer to fuel ratio. The large size of the error bars relative to the absolute dynamic pressure P'_{rms} value is due to the low signal to noise ratio particularly in the case of the 1T mode.

When compared with Figure 6 this suggests that any contribution that depends on oxidizer to fuel ratio falls outside the primary acoustic modes of interest.

When comparing these results to those observed by Wanhainen et al (1966), it is clear that the same trend in stability is not observed. In the warm GH2 case a higher oxidizer to fuel ratio lead to increased combustion stability. This is unlike the Wanhainen et al (1966) case where higher oxidizer to fuel ratios lead to instability occurring at higher hydrogen temperatures and is therefore considered less stable than lower oxidizer to fuel ratios. However, it is unlikely that the significant differences in hardware, hydrogen temperature and stability rating technique have

allowed for reasonable comparison to be made, and thus a difference in findings is not suppressing.

3.2. Effect of Injection Velocity Ratio

The relationship between injection velocity ratio for the high frequency domain vs dynamic stability is presented in Figure 9 The relationship for the 1T and 1L modes was also investigated but found to have no dependence on injection velocity ratio as in the oxidizer to fuel ratio case.

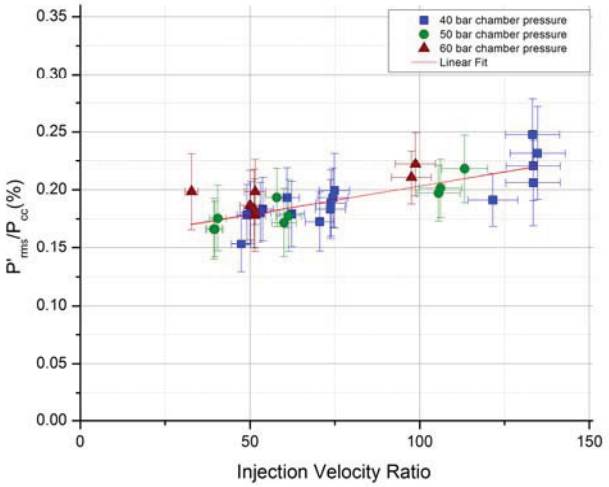

Figure 9. Injection velocity ratio vs. normalized dynamic chamber pressure RMS for the high frequency domain.

A line of best fit was also applied here and was found to have a positive gradient again the line was found to be significant (greater than 95%) with respect to the null hypothesis case. The R^2 value remained relatively constant (0.57) with respect to the line of best fit for oxidizer to fuel ratio.

3.3. Effect of Momentum Flux Ratio

Momentum Flux ratio was also investigated to complement the previously discussed Injection velocity ratio. The relationship between dynamic pressure in the high frequency domain and momentum flux ratio is presented in Figure 10.

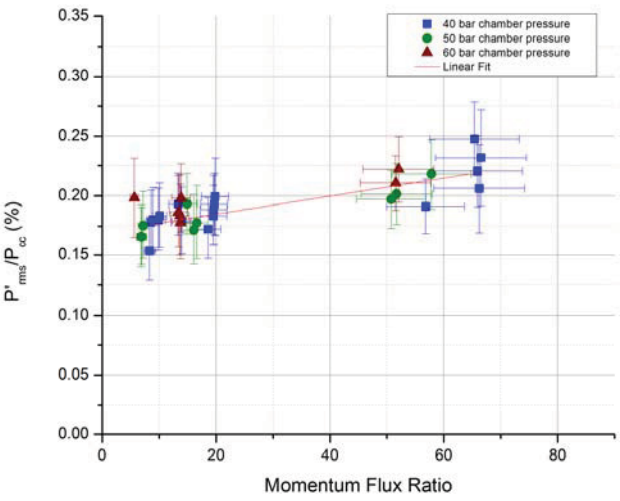

Figure 10. Momentum flux ratio vs. normalized dynamic chamber pressure RMS for the high frequency domain

The range of momentum flux ratios observed is large compared to the normal operation of a flight engine which is generally below 20.

The line of best fit resulted in a positive gradient like that observed for Injection velocity ratio and maintained the significance of those trends previously described. The R^2 value (0.61) was similar to those in the previous cases.

3.4. Secondary Hydrogen Dome Mode Effects.

The results presented thus far have focused on data sets with removed contribution of an acoustic mode originating in the secondary hydrogen dome. The effects of the dome mode in particular on the 1L combustion chamber mode require further investigation to validate the removal of its contribution for characterization of the relationship between injection conditions and combustion stability.

Figure 11 shows both the scatterplot for injection velocity ratio before and after removal of the secondary dome mode contribution to the main combustion chamber spectra. Two things are immediately evident. Firstly the contribution of the secondary dome mode to the combustion chamber spectra accounts for a significant part of the dynamic pressure signal RMS. Secondly the contribution of the secondary dome mode to the combustion chamber spectra is not consistent in amplitude across all operation points.

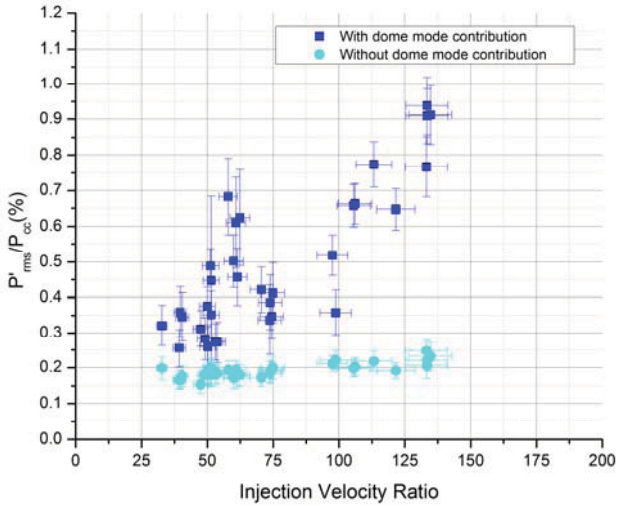

Figure 11: Effect of secondary dome mode filtering on normalized dynamic pressure RMS.

From these two observations it is reasonable to suggest that the secondary dome mode does not strongly couple with any other acoustic process or process that would lead to a further distribution in energy outside of the secondary hydrogen dome mode frequency band. If it did the influence of higher dome mode energy content should be observable in the filtered data. In support of this statement, Figure 12 displays the same plot with data from tests with the same configuration with one exception the inclusion of a baffle in the secondary dome. Although only

a few operational points are available from a limited number of tests it is clear that the large distribution with respect to dynamic chamber pressure energy pre-filtering is not observable and the energy values are similar to the post filtered data from the previous campaign.

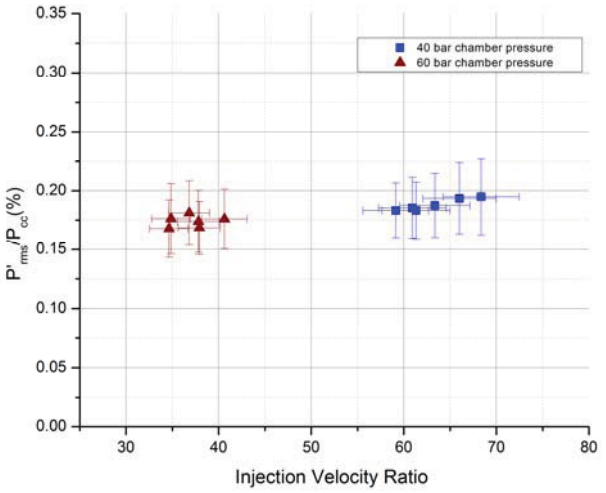

Figure 12: Injection velocity ratio vs. dynamic chamber pressure RMS for tests with secondary dome baffle.

In an attempt to account for the spread in dynamic chamber pressure prior to filtering the pressure drop across the secondary chamber as well as mass flow rates and energy content (P'_{rms}) within the dome were investigated. An increase in pressure drop across the injector of secondary hydrogen did appear to reduce the maximum amount of energy that was transmitted (Figure 13).

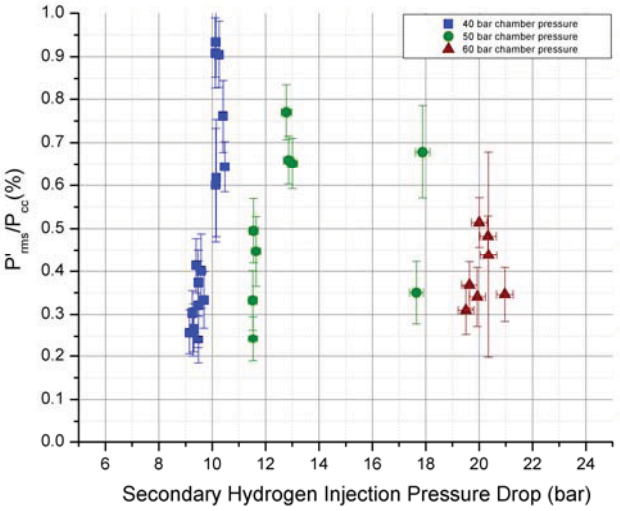

Figure 13. Secondary hydrogen injection pressure drop vs. dynamic chamber pressure RMS.

However, given the nature of secondary hydrogen injection and single hardware configuration this parameter cannot be separated from combustion chamber pressure, secondary dome pressure, and secondary hydrogen mass flow rates making any relationship difficult to identify. One thing can be said with certainty; the dynamic hydrogen dome pressure oscillation energy (P'_{rms} secondary hydrogen dome) was independent of all operating conditions and maintained a relatively constant value. It is also interesting to note that the normalized dynamic RMS of secondary hydrogen dome pressure was significantly higher (around 4.5 to 5 % of secondary hydrogen dome pressure) than that of the combustion chamber (less than 1% of combustion chamber pressure) when the acoustic mode was included in both.

When investigating the previously discussed spread with respect to chamber stability it is important to keep in mind that the hydrogen injected through the secondary dome takes a small if any part in the combustion process. This is because it is spatially removed from the oxygen jets and the combustion chamber runs at a low overall oxidizer to fuel ratio. If the secondary hydrogen did take part in the combustion process then the flow perturbation due to the acoustic mode in the dome would likely have a strong effect on combustion rate and it is unlikely that filtering of this mode would have had the same effect on the scatter plots.

4. CONCLUSION

The relationships investigated in this paper for GH2 over a range of combustion chamber pressures and injection conditions show trends with a significance of more than 95% with respect to a null hypothesis of zero gradient. The trend lines observed in oxidizer to fuel ratio and injection velocity ratio are in contrast with the observations made by Wanhainen et al in 1966 using the temperature ramping stability method. However, the trend lines observed exhibit a very low gradient value resulting in little significant dependence when comparing dynamic chamber pressure energy with injection conditions. This is not a surprising conclusion as warm co-axial hydrogen and LOx injection is known to be highly stable. The high level of stability of the combustion chamber is well represented with P'_{rms} values of less than 0.2% of combustion chamber pressure when the influence from an acoustic mode in the secondary dome is removed.

The natural progression of this work would be to investigate stability with cryogenic hydrogen (LH2) which is known to become unstable with decreasing temperature. This is possible at the test facility P8 where the GH2 investigations were undertaken. The test matrix can then be extended to investigate the effects of forcing at both ambient GH2 and at cryogenic LH2 temperatures as is the original intention of the 'BKH' design.

The removal of secondary dome modes by the installation of a baffle allows examination of the effect of injection conditions on chamber stability with minimal data processing required. The test matrix regarding GH2 operating conditions with baffle will require an extension if it is to be used as a baseline for extension of the work into the LH2 domain. However, if this is not possible due to limited resources the filtered results presented here can be used as a baseline as long as the effects of additional processing such as the removal of the secondary dome mode are kept in mind.

References

[1] D. T. Harrje and F. H. Reardon, "Liquid propellant rocket combustion instability." Washington, D.C.: National Aeronautics and Space Administration, 1972.

[2] V. Yang and W. Anderson, "Liquid rocket engine combustion instability," in Progress in Astronautics and Aeronautics, vol. 169, P. Zarchan, Ed. Washington, DC: American Institute of Aeronautics and Astronautics, 1995.

[3] R. Lecourt and R. Foucaud, "Experiments on Stability of Liquid Propellant Rocket Motors," presented at AIAA/SAE/ASME/ASEE 23rd Joint Propulsion Conference, San Diego, California, 1987.

[4] B. Knapp and M. Oschwald, "High speed visualization of flame response in a LOx/H2 combustion chamber during external excitation," presented at 12th International Symposium on Flow Visualization, Gottingen, Germany, 2006.

[5] C. Rey, S. Ducruix, F. Richecoeur, P. Scouflaire, L. Vingert, and S. Candel, "High Frequency Combustion Instabilities Associated with Collective Interactions in Liquid Propulsion," presented at 40th AIAA/ASME/SAE/ASEE Joint Propulsion Conference & Exhibit, Fort Lauderdale, Florida, 2004.

[6] John P. Wanhainen, Harold C. Parish, and E. Willam Conrad, “Effect of propellant injection velocity on screech in 20 000-Pound hydrogen-oxygen rocket engine,” NASA TN D-3373, April 1966.

[7] J. Hardi, M. Oschwald, B. Dally, “Acoustic characterisation of a rectangular rocket combustor with LOx/H_2 propellants”, Proceedings 4th EUCASS Conference (2011).

[8] M. F. Heidmann and P. R. Wieber, "Analysis of frequency response characteristics of propellant vaporization," Lewis Research Centre, National Aeronautics and Space Administration, Cleveland, Ohio NASA TN D-3749, 1966.